

ORIGINAL ARTICLE

Matrix degradation and cell proliferation are coupled to promote invasion and escape from an engineered human breast microtumor

Emann M. Rabie^{1,2}, Sherry X. Zhang³, Andreas P. Kourouklis³, A. Nihan Kilinc³, Allison K. Simi³, Derek C. Radisky⁴, Joe Tien^{5,6,*}, and Celeste M. Nelson^{2,3,*}

¹Rutgers Robert Wood Johnson Medical School, Piscataway, NJ, USA, ²Department of Molecular Biology, Princeton University, Princeton, NJ, USA, ³Department of Chemical & Biological Engineering, Princeton University, Princeton, NJ, USA, ⁴Department of Cancer Biology, Mayo Clinic, Jacksonville, FL, USA, ⁵Department of Biomedical Engineering, Boston University, Boston, MA, USA, and ⁶Division of Materials Science and Engineering, Boston University, Boston, MA, USA

*Corresponding authors. E-mail: jtien@bu.edu and celesten@princeton.edu

Abstract

Metastasis, the leading cause of mortality in cancer patients, depends upon the ability of cancer cells to invade into the extracellular matrix that surrounds the primary tumor and to escape into the vasculature. To investigate the features of the microenvironment that regulate invasion and escape, we generated solid microtumors of MDA-MB-231 human breast carcinoma cells within gels of type I collagen. The microtumors were formed at defined distances adjacent to an empty cavity, which served as an artificial vessel into which the constituent tumor cells could escape. To define the relative contributions of matrix degradation and cell proliferation on invasion and escape, we used pharmacological approaches to block the activity of matrix metalloproteinases (MMPs) or to arrest the cell cycle. We found that blocking MMP activity prevents both invasion and escape of the breast cancer cells. Surprisingly, blocking proliferation increases the rate of invasion but has no effect on that of escape. We found that arresting the cell cycle increases the expression of MMPs, consistent with the increased rate of invasion. To gain additional insight into the role of cell proliferation in the invasion process, we generated microtumors from cells that express the fluorescent ubiquitination-based cell cycle indicator. We found that the cells that initiate invasions are preferentially quiescent, whereas cell proliferation is associated with the extension of invasions. These data suggest that matrix degradation and cell proliferation are coupled during the invasion and escape of human breast cancer cells and highlight the critical role of matrix proteolysis in governing tumor phenotype.

Key words: mechanics; tumor engineering; physical oncology

INSIGHT BOX

Invasion and intravasation, early steps in the metastatic cascade, are critical for subsequent dissemination of cancer cells. The challenges of directly visualizing these steps have hindered our understanding of the relative roles of matrix degradation and cell proliferation during the intravasation process. This work uses 3D microtumor aggregates separated from an empty cavity, which serves as an artificial vessel, to provide insight into the effects of matrix degradation and cell proliferation on tumor intravasation. In particular, this work highlights the essential role played by matrix proteolysis in tumor invasion and intravasation.

INTRODUCTION

The escape and subsequent dissemination of cancer cells from a primary tumor to distant sites depend upon their ability to invade and migrate through the surrounding extracellular matrix (ECM). Cancer cell invasion and intravasation into the nearby lymphatic or circulatory system are influenced by many factors, including ECM concentration, pore size, and degradability. Different modes of single-cell invasion have been extensively characterized, particularly those that rely on amoeboid or mesenchymal motility [1]. Amoeboid motility involves a series of contractions and expansions of the cell body that allow the cancer cell to migrate without degrading its surrounding ECM [2]. In contrast, mesenchymal motility requires cells to proteolytically degrade the ECM using enzymes such as matrix metalloproteinases (MMPs) [2]. When intercellular adhesions are maintained, cells invade collectively as multicellular chains. This type of migration is dependent on mesenchymal motility, where leader cells extend actin-rich protrusions and continually degrade the ECM through MMP-mediated proteolysis to allow extension into the surrounding tissue [3]. MMP-mediated proteolysis has been found to increase tumor angiogenesis, invasion, and metastasis [4]. MMPs promote invasion and metastasis by cleaving E-cadherin, which can result in epithelial-mesenchymal transition (EMT) and increased tumor cell motility [5]. Upregulation of MMPs in breast cancer has been associated with genomic instability, shorter relapse-free survival, and decreased overall survival [6, 7].

In addition to matrix degradation, abnormally high rates of cell proliferation are a common characteristic of tumors. In principle, elevated proliferation can increase the likelihood of future metastases by increasing the number of potentially invasive cells [8, 9]. Even so, several studies have suggested that highly proliferative cells have decreased invasive capacity compared with nonproliferating cells, and must be arrested in the G1 phase of the cell cycle in order to invade through the ECM [10–13]. The switch from a proliferative state to a G0/G1 cell cycle-arrested state has been associated with an EMT phenotype, an upregulation of genes involved in actin cytoskeletal reorganization and basement membrane invasion [12]. At the same time, downregulation of genes associated with proliferation, such as cyclin D1/E, has been correlated with increased invasiveness in patient samples [14]. Consistently, clinical and preclinical studies have found that conventional chemotherapy, which targets growth of the cells in the primary tumor, is associated with an increase in metastasis in some patients and animal models [15–17]. Therefore, although elevated proliferation rates are characteristic of many types of cancer, inhibiting proliferation may inadvertently promote cancer progression.

Mouse models of cancer have been used to investigate the different factors involved in tumor cell invasion [18–21]. It is difficult to directly image intravasation and escape in these systems; vascular escape is usually detected indirectly by capturing circulating tumor cells or by measuring the metastatic burden in one or more target organs [18, 22]. Therefore, our understanding of the mechanisms of invasion and escape has primarily resulted from studies using culture models, including transwell assays, tumor spheroids, artificial microvessels, and microfluidic devices [18, 23]. Although devices have been developed to incorporate vascular or interstitial flow, many fail to combine the flow with the 3D cellular organization and microenvironment within and around a tumor [23, 24].

We previously described a culture model that allows for the direct visualization of tumor cell invasion [25, 26]. This system, which consists of a microtumor in the form of an engineered aggregate of human breast cancer cells embedded within a 3D collagen matrix, was recently modified to incorporate an empty cavity located adjacent to the microtumors into which invasive cells can escape [27, 28]. Here, we used this engineered microtumor model to investigate the relative roles of matrix degradation and cancer cell proliferation in invasion and escape in the absence of the chemical and biological contributions of endothelial and other stromal cells. The microtumors were comprised of MDA-MB-231 cells, a cell line commonly used in studies of invasion and other steps of the metastatic cascade in culture. We found that the ability of the microtumor to continually degrade the matrix is essential for escape of cancer cells into the empty cavity, whereas proliferation is not necessary for invasion or escape. In fact, the majority of cells that initiate invasion are quiescent, and blocking proliferation increases the rate of invasion. Cell proliferation is instead associated with the growth and extension of invading collectives. These observations suggest that although invasion and escape depend on proteolysis, proliferation can enhance the persistence of existing invasions to allow for a more aggressive phenotype. Taken together, our data show that matrix degradation and proliferation work synergistically to influence cancer progression by promoting the initiation and growth of invasions.

MATERIALS AND METHODS

Cell culture and reagents

MDA-MB-231 human breast cancer cells (ATCC), passaged at a 1:4 ratio and used between passages 3–15, were cultured in DMEM/F12 medium (Hyclone) supplemented with 10% heat-inactivated fetal bovine serum (FBS, lot F17089; Atlanta

Biologicals) and 50 µg/ml gentamicin (Gibco). The following reagents were used at the indicated concentrations: GM6001 (40 µM; Calbiochem), mimosine (400 µM; Sigma) and aphidicolin (2 µM; Sigma).

Plasmid transfection

MDA-MB-231 cells were transfected with pBOB-EF1-FastFUCCI-Puro plasmid (Addgene plasmid #86849) using FuGENE HD Transfection Reagent (Promega). FuGENE and the plasmid were mixed with Opti-MEM medium (3:1 FuGENE reagent:DNA ratio), incubated for 10 min at room temperature, and then added directly to culture medium. Cells stably expressing the plasmid were generated by pooling several clones that were selected using puromycin (2.5 µg/ml; Sigma) for 2–3 weeks.

Formation of 3D microtumors

Microtumors consisted of aggregates of MDA-MB-231 cells surrounded by a collagen gel within a channel of polydimethylsiloxane (PDMS), and were constructed by modifying a previously described technique [25–28]. Briefly, acid-extracted bovine type I collagen (4.9 mg/ml; lot# 210090, Koken) was neutralized to pH 9–9.5 using 0.2 M NaOH and mixed with 10× Hank's balanced salt solution (Invitrogen) and cell culture medium to obtain a solution with final collagen and FBS concentrations of 3.9 mg/ml and 0.4%, respectively. The collagen solution (10–15 µl) was introduced into a PDMS channel that contained two opposing 120 µm diameter needles (Seirin) and then allowed to gel for 25 min at 37°C (Fig. 1A). After gelation, the needles were removed to generate two empty cavities opposing each other. The resulting gels were conditioned by adding ~50 µl culture medium to one side and allowing it to percolate through the gel for at least 1 h prior to seeding cells. To seed the microtumors, we introduced ~50 µl of a concentrated cell suspension (2–3 million cells in 1 ml) to one side of the gel. Cells flowed into the adjacent empty cavity by advection and completely filled the cavity within 15 min of introducing the cell suspension. Once the cavity was seeded, the cell suspension was replaced with culture medium and the microtumors were incubated for 2 days at 37°C, with the culture medium replaced every 10–14 h. The microtumors were then exposed to flow by placing a PDMS spacer (7–8 mm high, with an 8 mm diameter hole) on the well of the empty cavity, and filling the well and hole in the spacer with culture medium. The flow speed (~1 µm/s) was measured as previously described [29] and was similar to values obtained *in vivo* [30] and in computational models of similar microtumors *in vitro* [27, 28]. Samples were monitored and fed once every 10–14 h, with ~60 µl of culture medium added to the stack and ~60 µl removed from the downstream well. Samples were imaged once per day using a Hamamatsu camera attached to a Nikon Ti-U inverted microscope at 10× magnification in air.

Measurement of gel permeability

To measure the permeability of the collagen gel, we used a similar procedure as described above, but without needles, to generate a solid collagen gel. A PDMS stack was used to apply a pressure difference across the gel, and the volume of culture medium that flowed through the gel was measured 2–4 h later. The permeability of the gel ($\kappa = 0.053 \pm 0.0048 \mu\text{m}^2$) was calculated using Darcy's Law, $Q = \frac{\kappa A}{\mu L} \Delta P$, where Q is the total discharge or flow rate of the medium, κ is the permeability, A is

the cross-sectional area of the collagen gel (0.7–1.1 mm²), ΔP is the pressure difference across the gel (0.8–1.5 cm H₂O), μ is the viscosity of culture medium (0.72 mPa s) and L is the length of the gel (6–7.5 mm).

Analysis of proliferation

Proliferation was assessed by quantifying the percentage of EdU-positive cells using the Click-iT EdU Alexa Fluor 594 Kit (Thermo Fisher Scientific). Samples were exposed to EdU for 2 h and then immediately fixed with 4% paraformaldehyde in phosphate-buffered saline (PBS) before applying the Click-iT cocktail reagent.

Imaging and image analysis

Phase-contrast images of the microtumors were collected using a Nikon Ti-U inverted microscope at 10× magnification. The tumor-to-cavity distance was measured as the smallest distance from any tumor cell to the tip of the empty cavity, starting at day 2 of culture. Microtumors were considered to have invaded when one cell body protruded from the surface of the aggregate into the surrounding collagen; this invasion was classified as an initial invasion or as an initial invading cell, depending on whether it was multicellular or unicellular. Microtumors were considered to have escaped when at least one cell body was observed within the empty cavity. Invasions that failed to increase in length after they were first detected were considered to be static invasions, whereas those that increased in length were considered to be extending invasions. Leader cells were considered to be the cells at the tip of an existing invasion. The diameter of each microtumor was measured at a distance of 200 µm plus the initial (day 2 after seeding) tumor-to-cavity distance away from the tip of the empty cavity.

Quantitative reverse transcriptase polymerase chain reaction analysis

Microtumors were incubated with a solution of 2.5 mg/ml collagenase (Sigma) for 5–10 min prior to isolating RNA using TRIzol (Invitrogen). Isolated RNA was used to generate complementary DNA (cDNA) using a Verso cDNA Synthesis Kit (Thermo Scientific). Transcript levels were measured using an Applied Biosystems Step One Plus instrument and iTaq Universal SYBR Green SuperMix (Bio-Rad). Melt-curve analysis was used to verify the amplification of only one polymerase chain reaction (PCR) product. The expression level of each gene was normalized to that of 18S ribosomal RNA in the same sample. Primers were designed using PrimerQuest (IDT) and verified for specificity using BLAST (Supplementary Table S1). Experiments were performed on at least three independent biological replicates with at least 10 microtumors per treatment condition per experiment.

Statistical analysis

All statistical analysis was performed using Prism version 8 (Graphpad). Comparisons of invasion and escape kinetics were performed using the log-rank (Mantel–Cox) test with hazard ratios calculated by the Mantel–Haenszel method. Comparisons of microtumor diameter and tumor-to-cavity distance used repeated measures two-way analysis of variance (ANOVA) with Sidak's *post hoc* test (for two groups) and Tukey's *post hoc* test (for more than two groups). Student's *t*-test was used

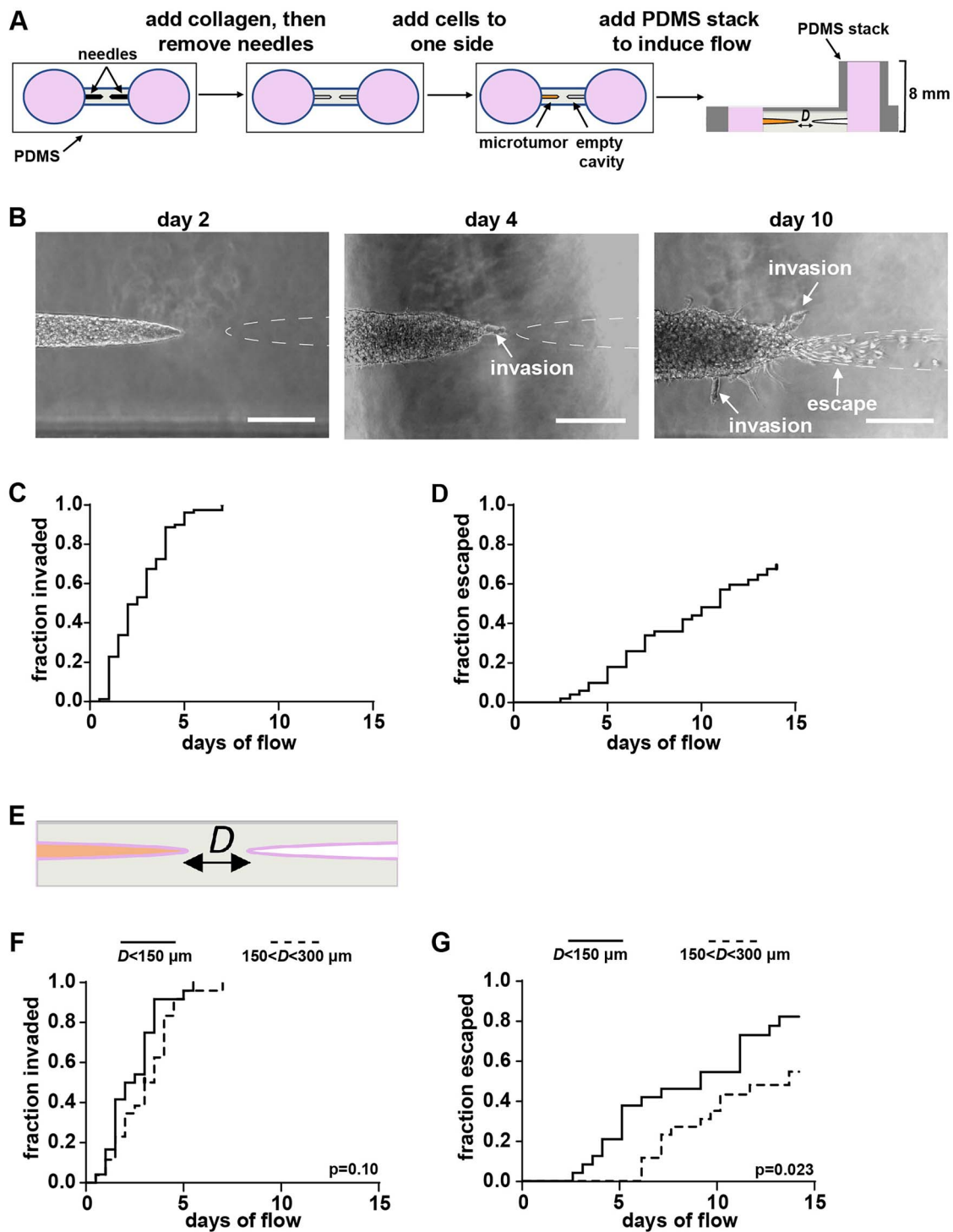


Figure 1. Three-dimensional microtumor model to study invasion and escape. (A) Schematic of 3D microtumor. (B) Phase-contrast images of microtumors showing invasion and escape. Kaplan-Meier plots of (C) invasion ($n = 83$) and (D) escape ($n = 50$). (E) Schematic of microtumors indicating initial tumor-to-cavity distance D . Kaplan-Meier plots of (F) invasion ($P = 0.10$) and (G) escape [$P = 0.023$, hazard ratio (HR): 2.3, 95% CI: 1.1–4.8] for microtumors with $D < 150 \mu\text{m}$ ($n = 24$) or $150 < D < 300 \mu\text{m}$ ($n = 26$). Scale bars, 200 μm .

for comparisons of percent EdU⁺ cells. Welch's *t*-test was used for comparisons of relative MMP expression. Group and pairwise comparisons of cell cycle analysis used one-way ANOVA with Tukey's *post hoc* test, respectively. All experiments

were performed using at least three independent biological replicates. All reported *P*-values have been adjusted for any multiple comparisons, and a *P*-value < 0.05 was considered to be statistically significant.

RESULTS

Tumor-to-cavity distance has no effect on invasion, but controls the rate of escape

Although it is well established that matrix degradation plays a role in local invasion, the effects of matrix degradation on the process of escape have not been reported. To parse the effects of matrix degradation on invasion and subsequent escape in the absence of contributions from endothelial cells, we generated microtumors comprised of MDA-MB-231 human breast cancer cells that were embedded within a type I collagen gel (Fig. 1A). Briefly, two needles were used to generate blind-ended cavities within the gel. A high concentration of suspended cells was then used to seed one of the cavities to produce the microtumor [25, 26]. Tumor cells encounter either interstitial, lymphatic, or vascular fluid flow during metastasis to distant organs. Interstitial hypertension, which results in an outward flow of interstitial fluid from the tumor core into the periphery, has been shown to suppress invasion in culture [25, 29]. We previously found that microtumors fail to invade in the absence of flow from the boundary of the tumor to the tumor bulk [25, 29]. Therefore, to permit invasion into the surrounding microenvironment, we exposed microtumors to interstitial flow directed at the tumor 2 days after seeding [25, 26] (Fig. 1B). After 4 days of flow (6 days after seeding), almost all microtumors had formed invasions (Fig. 1C). After 14 days of flow (16 days after seeding), at least one cell from three-quarters of the microtumors had escaped into the empty cavity (Fig. 1D).

Since the migration of tumor cells is one process that allows for escape, and since tumors are surrounded by vessels located at varying distances in the microenvironment, we examined the effect of the distance between the microtumor and the empty cavity on the kinetics of invasion and escape. Analyses of tumors of the breast as well as head-and-neck cancers have revealed that intercapillary distances greater than ~ 150 μm can result in the development of hypoxia and necrosis [31, 32]. In addition, analysis of cervical cancer has shown that the mean tumor–intercapillary distance is ~ 300 μm , regardless of clinical stage [33]. Therefore, we varied the initial tumor-to-cavity distance from <150 to ~ 300 μm and monitored invasion and escape. We segregated the microtumors into those in which the distance to the cavity was <150 μm and those with distances between 150 and 300 μm (Fig. 1E). Regardless of the initial tumor-to-cavity distance, nearly all microtumors invaded into the surrounding collagen within 4 days of the application of flow (6 days after seeding) (Fig. 1F). Escape, however, occurred faster in microtumors located closer to the cavity (Fig. 1G). These data suggest that, in the absence of endothelial cells, the rate-limiting step for escape is migration through the ECM between the primary microtumor and the escape cavity.

Matrix degradation is required for invasion and escape

To determine the effects of matrix degradation on invasion and escape, we matched microtumors based on initial tumor-to-cavity distance (Supplementary Fig. S1A) and treated them with vehicle control (0.1% v/v DMSO) or the broad-spectrum MMP inhibitor GM6001 (40 μM) starting on the day that flow was applied (2 days after seeding) (Fig. 2A and B). Compared with controls, GM6001-treated microtumors neither invaded nor escaped (Fig. 2C and D). These data suggest that tumor growth alone is insufficient for tumor cells to escape, and that instead

matrix proteolysis is essential for invasion and escape through a collagen-rich microenvironment.

Since invasion precedes escape, it is possible that the effects of GM6001 on escape result solely from its suppression of invasion. To test this possibility, we next examined whether matrix degradation is required for the escape of microtumors that have already invaded. We generated distance-matched microtumors (Supplementary Fig. S1B), cultured them in the presence of flow for 4 days to promote invasion, confirmed that the tumor-to-cavity distance distributions remained matched after 4 days and only then treated the microtumors with vehicle control or GM6001 (Fig. 2E). Even when MMP activity was only inhibited after invasions had already formed (Fig. 2F), we found that microtumors still failed to escape (Fig. 2G). These results suggest that continuous degradation of the surrounding matrix is required for progressive invasion and escape.

Inhibiting matrix degradation decreases the proliferation and growth of microtumors

Phase-contrast images revealed that the diameter of the microtumors increased significantly over the 2 weeks of culture (Fig. 3A). Curiously, treatment with GM6001 led to a reduction in the diameter of the microtumors (Fig. 3B). These data suggest that inhibiting MMP-associated proteolysis might also affect the proliferation of the cancer cells within the microtumor.

To test this hypothesis, we carried out an EdU-incorporation assay to detect DNA synthesis in the microtumors. We found that microtumors treated with GM6001 showed a reduction in EdU-positive cells (Fig. 3C), consistent with the decrease in their diameters relative to controls. This decrease in proliferation in the presence of GM6001 is also consistent with previous work showing that GM6001 reduces proliferation of fibroblasts [34]. It remains unclear why inhibiting MMP activity decreases proliferation of MDA-MB-231 cells in the microtumors; the reduction in proliferation that we observed here could be a result of confinement [35] or the inability of the microtumor to expand into the surrounding collagen rather than a direct effect of GM6001 itself.

Inhibiting proliferation accelerates invasion, but does not affect escape

To decouple the effects of MMP inhibition on proliferation and the kinetics of escape, we next examined whether proliferation is required for invasion and escape. To block proliferation, we treated microtumors with mimosine, a DNA replication inhibitor that arrests cells in the G1 phase of the cell cycle by inhibiting deoxyribonucleotide metabolism and preventing the formation of new replication forks [36] (Fig. 4A and B). One day prior to the start of flow (1 day after seeding), microtumors were distance-matched (Supplementary Fig. S1C) and treated with either vehicle control (3% v/v PBS) or mimosine (400 μM). We used EdU analysis to assess proliferation 2 days later (1 day of flow). This assay confirmed that treatment with mimosine for 48 h blocked proliferation of the cells within the microtumors nearly completely (Supplementary Fig. S2). Surprisingly, we found that mimosine-treated microtumors formed invasions earlier than did controls (Fig. 4C), but showed no overall difference in the kinetics of escape (Fig. 4D). Although they invaded earlier than controls, the migration rate of mimosine-treated microtumors decreased over time (Fig. 4E), which could explain the paradoxical escape kinetics. As expected, treatment with mimosine caused a decrease in the growth of the microtumors as compared with vehicle controls (Fig. 4F). These observations are consistent

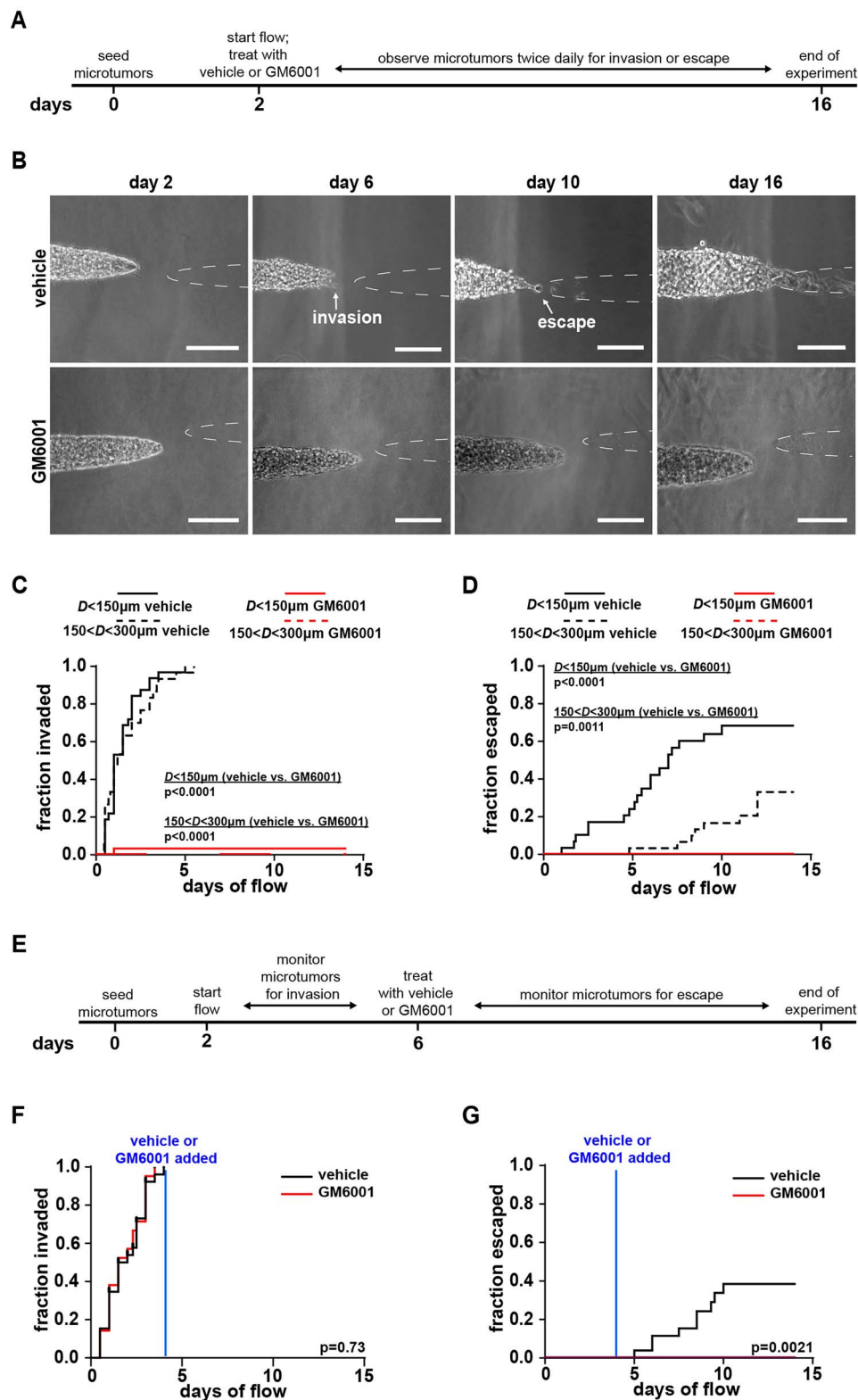


Figure 2. Inhibiting MMP activity prevents invasion and escape. (A) Timeline of experiment. (B) Phase-contrast images of microtumors treated with vehicle control (DMSO) (top panel) or the MMP inhibitor GM6001 (bottom panel) starting on the day of flow (2 days after seeding). Kaplan-Meier plots of (C) invasion [$P < 0.0001$, HR: 25.9, 95% CI: 11.8–57.1 for $D < 150 \mu\text{m}$ vehicle control ($n = 32$) vs. GM6001 ($n = 30$); $P < 0.0001$, HR: 27.9, 95% CI: 12.4–62.7 for $150 < D < 300 \mu\text{m}$ vehicle control ($n = 30$) vs. GM6001 ($n = 27$)] and (D) escape [$P < 0.0001$, HR: 13.1, 95% CI: 5.5–31 for $D < 150 \mu\text{m}$ vehicle control ($n = 32$) vs. GM6001 ($n = 30$); $P = 0.0011$, HR: 9.1, 95% CI: 2.4–34.1 for $150 < D < 300 \mu\text{m}$ vehicle control ($n = 30$) vs. GM6001 ($n = 30$)]. (E) Timeline of experiment. Kaplan-Meier plots of (F) invasion ($P = 0.73$) and (G) escape ($P = 0.0021$, HR: 8.0, 95% CI: 2.1–29.8) for microtumors treated with vehicle control ($n = 26$) or GM6001 ($n = 21$). Scale bars, 200 μm . HR, hazard ratio.

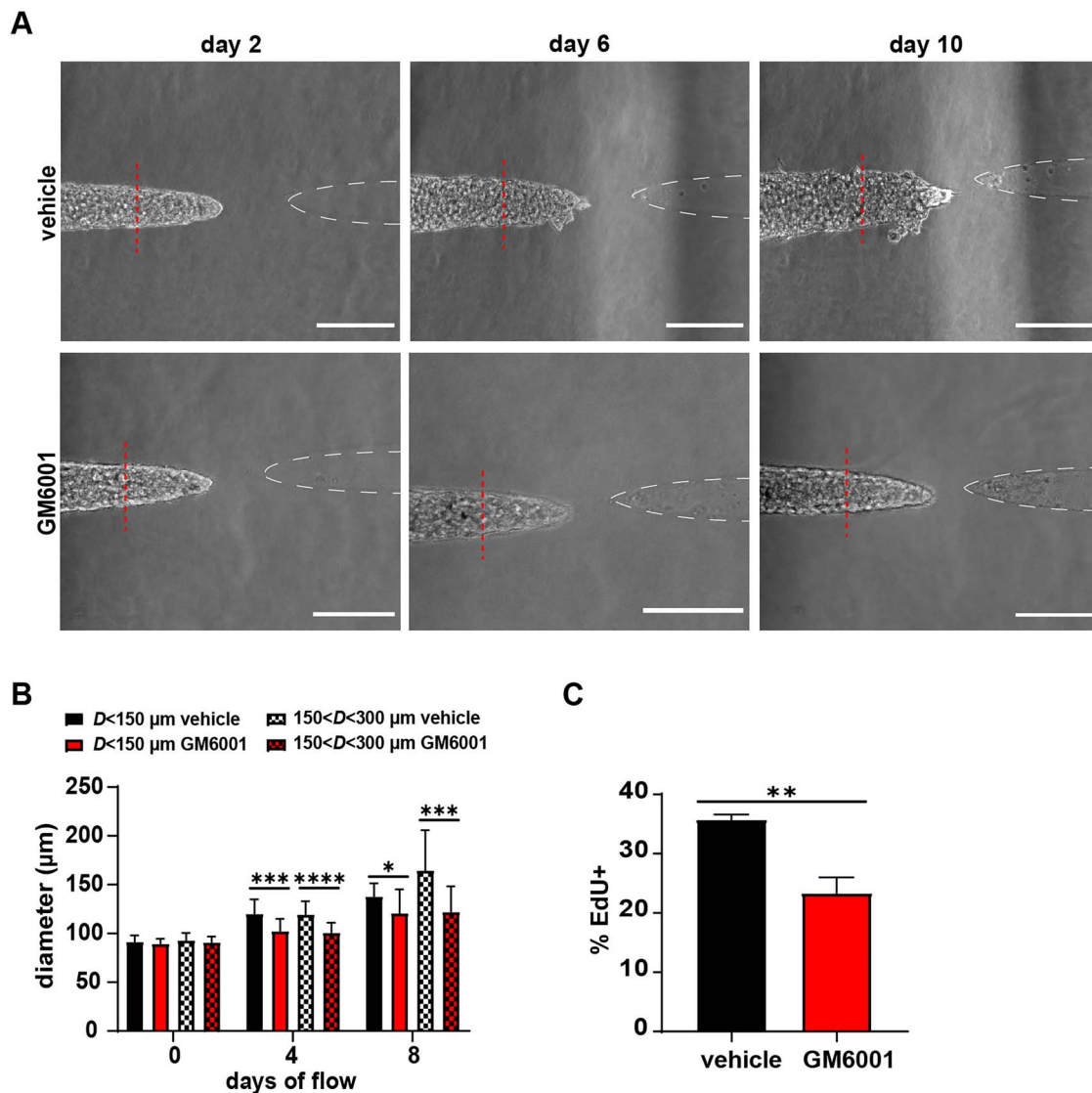


Figure 3. Inhibiting MMP activity reduces growth and proliferation of microtumors. (A) Phase-contrast images of microtumors treated with vehicle control (DMSO) (top panel) or GM6001 (bottom panel) starting on the day of flow. Quantification of (B) diameters (measured at dotted line) and (C) proliferation of microtumors treated with vehicle control or GM6001. Shown are mean \pm SD of three to five independent experiments. * $P < 0.05$, ** $P < 0.01$, *** $P < 0.001$, **** $P < 0.0001$ using two-way ANOVA with Tukey's post hoc test (B) or Student's *t*-test (C). Scale bars, 200 μm .

with other studies that have shown that exposure to mimosine reduces cell migration [37]. Therefore, although mimosine-treated microtumors invade earlier than controls, their migration rates decrease over time, which could explain why their escape kinetics do not differ from that of controls.

To determine whether these alterations in the invasion and escape kinetics were specific to mimosine, we treated microtumors with aphidicolin (Supplementary Fig. S3A and B), which prevents DNA replication by inhibiting DNA polymerases [36]. Unlike mimosine, aphidicolin does not affect cell migration, thus allowing the effects of proliferation and migration to be decoupled [38, 39]. As with the mimosine experiments, microtumors were distance-matched 1 day prior to application of flow (1 day after seeding) and treated with either vehicle control (0.01% v/v DMSO) or aphidicolin (2 μM) (Supplementary Fig. S3C). EdU analysis confirmed that treatment with aphidicolin for 48 h blocked proliferation of the cells within the microtumors (Supplementary Fig. S3D).

Similar to mimosine-treated microtumors, aphidicolin-treated microtumors formed invasions earlier than vehicle-treated microtumors (Supplementary Fig. S3E), but escaped with similar kinetics as controls (Supplementary Fig. S3F). These observations reveal that inhibiting proliferation hastens the initiation of invasions, but has no effect on the escape of microtumors through collagen-rich microenvironments.

Mimosine-treated microtumors upregulate expression of MMPs

It has been shown previously that exposure to mimosine can result in an increase in MMP activity [40]. To determine whether an increase in MMP expression could explain the faster invasion kinetics of mimosine-treated microtumors, we used quantitative reverse transcriptase PCR analysis to monitor MMP expression in microtumors in the presence or absence of mimosine. Previous work identified expression of >20 MMPs in MDA-MB-231

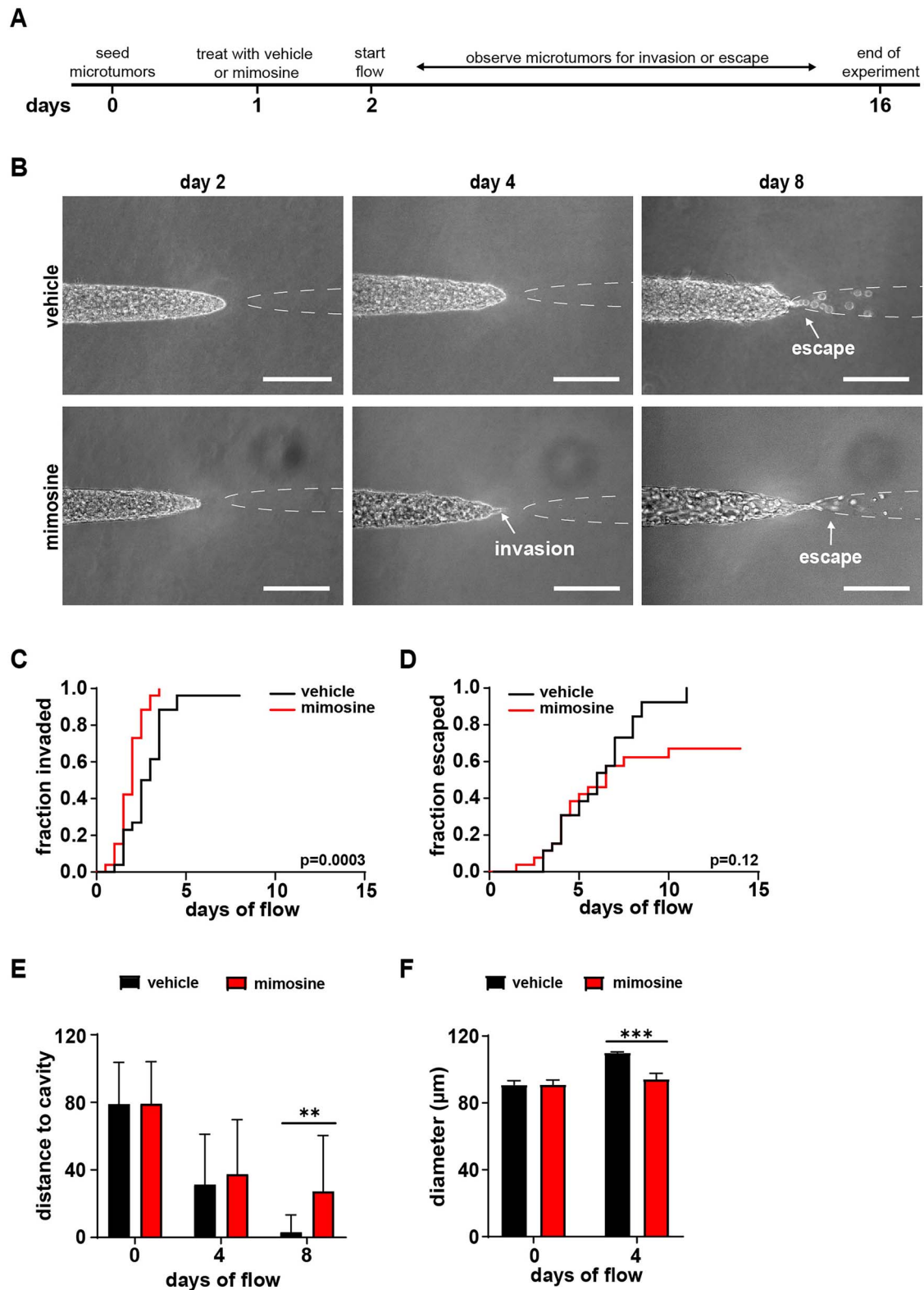


Figure 4. Inhibiting proliferation leads to earlier invasion. (A) Timeline of experiment. (B) Phase-contrast images of microtumors treated with vehicle control (PBS) (top panel) or the DNA replication inhibitor mimosine (bottom panel). Kaplan–Meier plots of (C) invasion ($P = 0.0003$, HR: 3.9, 95% CI: 1.9–8.1) and (D) escape ($P = 0.12$, HR: 0.6, 95% CI: 0.31–1.1) of microtumors treated with vehicle control ($n = 26$) or mimosine ($n = 26$). (E) Distance between the microtumor and the cavity at different days of flow for vehicle control- and mimosine-treated microtumors. (F) Diameters of microtumors in each group. Shown are mean \pm SD of three to four independent experiments. ** $P < 0.01$, *** $P < 0.001$ using two-way ANOVA with Sidak multiple comparisons test (E and F). Scale bars, 200 μm . HR, hazard ratio.

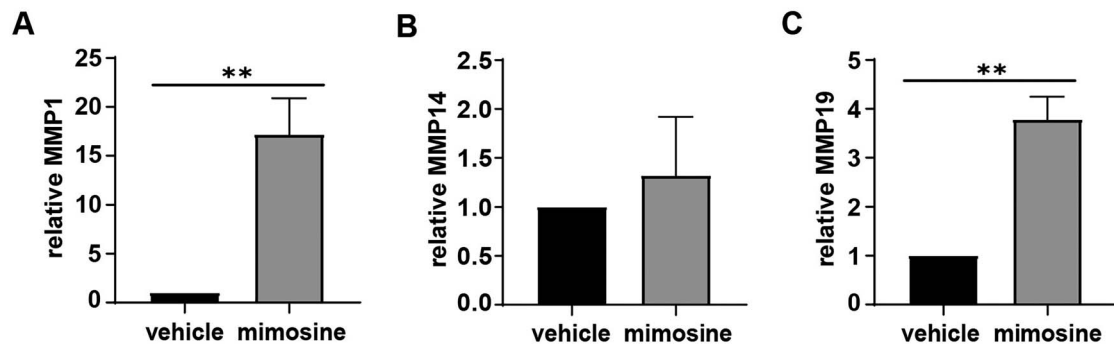


Figure 5. Mimosine-treated microtumors upregulate the expression of MMPs. Relative transcript levels of (A) MMP1, (B) MMP14, and (C) MMP19 in vehicle control- or mimosine-treated microtumors after 2 days of flow. Shown are mean \pm SD of four independent experiments. ** $P < 0.01$ using Welch's t-test.

cells at varying levels, with MMP1, 14, and 19 expressed at the highest levels [41]. We found that microtumors treated with mimosine upregulated the expression of MMP1 and MMP19, but we observed no apparent change in the expression of the transmembrane MMP14 (Fig. 5A–C). MMP1, a collagenase, is upregulated in human breast cancer tissues [42], promotes the growth and metastasis of cancer cells in mice [43], and is associated with shorter relapse-free survival [44]. Similarly, increased expression and activation of MMP19, a stromelysin, is associated with poor prognosis in patients with breast, lung, and colorectal cancer [44–46]. Although we found no change in the expression of MMP14, this transmembrane protease is also associated with metastasis and poor prognosis in breast cancer patients [47, 48]. Since MMP-mediated proteolysis is necessary for invasion of cells from the microtumors, these data suggest that the faster invasion kinetics in response to pharmacological inhibition of the cell cycle may be a result of increased MMP expression and activity.

Proliferation is not required for initiation of invasions, but is associated with their extension

Since inhibiting proliferation promoted invasion but had no effect on escape, we hypothesized that the cells that initiate invasions might be preferentially not proliferating. To test this hypothesis, we generated a stable line of MDA-MB-231 cells that expressed the fluorescent ubiquitination-based cell cycle indicator (FUCCI), which allows different stages of the cell cycle to be distinguished visually by labeling G0/G1 phase nuclei with red fluorescent protein and S/G2 phase nuclei with green fluorescent protein [49]. We generated microtumors comprised of FUCCI-expressing cells and tracked the cell cycle status of the population during invasion. Consistent with our hypothesis, we observed that the cell population that had the largest fraction of cells in the G0/G1 phase of the cell cycle were cells that initiated invasions (Fig. 6A–C). In other words, cells that initiate invasions are more likely than other cells to be quiescent. We next quantified whether the leading cell, i.e. the cell at the tip in an existing invasion, had a preferred cell cycle status. Although most leader cells were in the G0/G1 phase of the cell cycle, the percentage of leader cells in G0/G1 was similar to that of cells within the bulk microtumor (Fig. 6C). These data suggest that leader cells exhibit no preferred cell cycle phase relative to the tumor. It remains unclear, however, whether a cell in the leading position retains leader cell status over the multiday period required for extension and escape.

To determine whether proliferation is required for an invasion to continue to extend through the collagenous

microenvironment, we quantified the percentage of proliferating and nonproliferating cells within invasions that increased in length and compared that with invasions that remained static in size. Invasions that failed to increase in length after they were first detected were considered to be static invasions, whereas those that increased in length were considered to be extending invasions. We found that ~35% of the cells in extending invasions were proliferating, compared with only ~15% of the cells in static invasions (Fig. 6C). Statistical comparisons revealed that the entire tumor, extending invasions, and leader cells form one group, whereas the initial invasions and static invasions form a second group with a higher percentage of cells in G0/G1. The spatial heterogeneity in cell cycle status in untreated microtumors is consistent with our findings in mimosine-treated microtumors, which show that inhibiting proliferation hastens initiation of invasions, but that some level of proliferation is required to promote the extension of invasions.

DISCUSSION

The metastatic cascade is a series of processes initiated by local invasion through the basement membrane and surrounding ECM, followed by intravasation into the blood or lymphatic vasculature prior to dissemination to distant sites [50]. Since the density of the vasculature can vary, cancer cells must often stimulate the formation of new vessels or invade through a wide range of distances in the ECM prior to breaching the lumen of lymphatic or blood vessels. Investigating how the features of the microenvironment, including tumor-to-vascular separation distance, affect invasion and intravasation is important for understanding the early processes that influence metastasis. To address this problem, we engineered human breast microtumors that were exposed to fluid flow separated by a controllable distance from an empty cavity within a type I collagen gel (Fig. 1). We found that increasing the tumor-to-cavity separation distance does not affect the ability of the microtumor to invade, but alters the probability and kinetics of escape (Fig. 1). These data suggest that, in the absence of endothelial cells, migration through the matrix microenvironment is the rate-limiting step to escape. Given that biochemical and mechanical signaling from the stroma influence cancer cell migration and invasion [51–54], it will be interesting to determine the relative roles of different features of the microenvironment, including the vascular endothelium, on the rates of invasion and escape.

Consistent with the above, inhibiting MMP-mediated proteolysis reduces the rate of migration of the cells from the microtumor, preventing both invasion and escape (Fig. 2). Inhibiting matrix degradation in microtumors that have already invaded

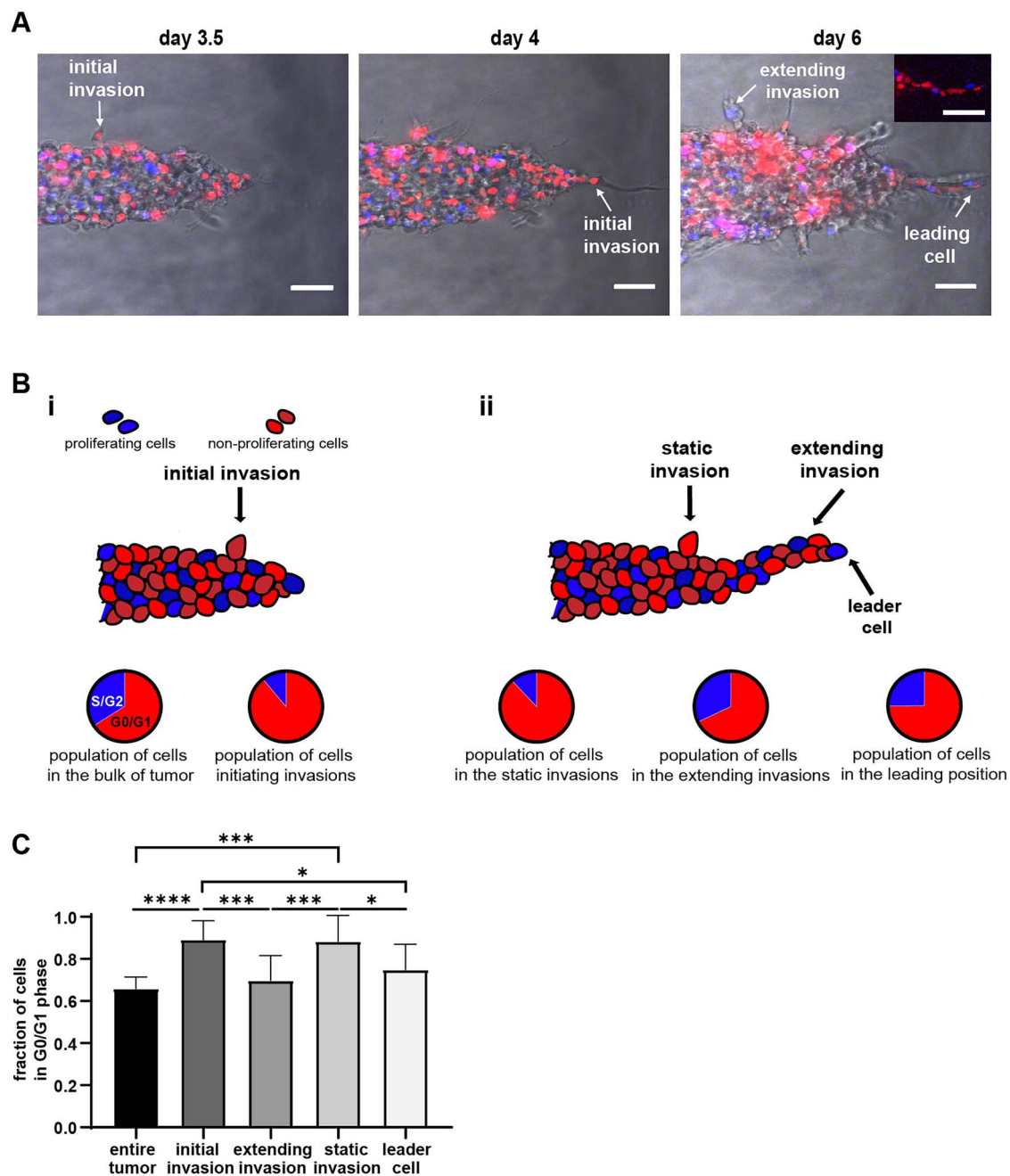


Figure 6. Proliferation is not required for initiation of invasions, but is associated with their extension. (A) Merged phase-contrast and fluorescence images of microtumors comprised of Fucci-expressing cells at different time points. Inset, confocal image of an extending invasion. (B) Schematic representing the different quantified invasion groups at (i) early and (ii) late time points in the microtumor. Pie charts represent the percentage of cells within each group. (C) Fraction of different cell populations in G0/G1 phase of the cell cycle. Shown are mean \pm SD of four independent experiments. * $P < 0.01$, *** $P < 0.001$, **** $P < 0.0001$ using one-way ANOVA with Tukey's post hoc test. Scale bar, 50 μ m.

also prevents escape (Fig. 2G). These data highlight the fact that, although it is necessary as the first step, invasion is not sufficient to ensure the occurrence of subsequent steps (e.g. intravasation) of the metastatic cascade [50]. Without continued proteolytic degradation of the surrounding matrix, invading tumor cells remain confined and are unable to extend and intravasate into the vasculature [55, 56].

Although inhibiting matrix degradation prevents invasion and escape in our system, which suggests MMP activity as a logical target for chemotherapy, clinical studies have found that

synthetic inhibitors of MMPs failed to reduce metastatic burden or improve survival [57–60]. The ability of tumor cells to compensate by switching from a mesenchymal, MMP-dependent mode of invasion to an amoeboid, MMP-independent mode has been proposed as an explanation for the failed clinical trials using MMP inhibitors [59, 61–63]. In our system, we did not observe this switching, which could be the result of the concentration of collagen that surrounds our microtumors. At the same time, clinical evaluation of MMP inhibitors has been conducted largely in late-stage cancer patients with severe metastasis, a setting

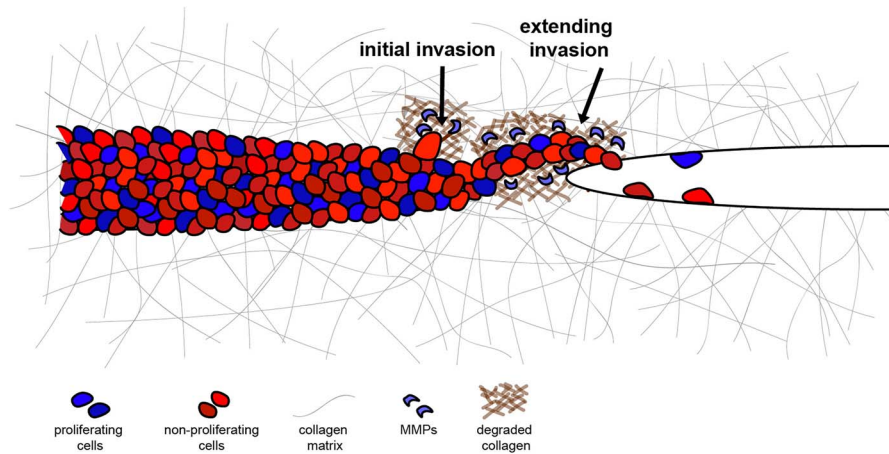


Figure 7. Summary of proposed mechanism of invasion and escape. MMP activity is required for the initiation and extension of invasions in the collagen matrix. Proliferation inhibits the initiation of invasions, but appears to be needed for the extension of invasions after they have formed.

where the effectiveness of these drugs is questionable [57–59]. To properly test whether inhibiting MMP activity may potentially reduce metastatic burden, these trials should be performed at earlier time points in patients with no metastatic disease [57–59]. In support of this concept, recent work in mouse models of breast cancer has shown that administering specific MMP inhibitors prior to the occurrence of any metastasis reduces metastatic burden and drastically improves survival [64]. These findings suggest that specific MMP inhibitors can potentially prevent metastatic disease and future recurrence if administered at earlier stages of tumor progression.

Since inhibiting matrix degradation resulted in a decrease in the proliferation of cells in the microtumors (Fig. 3), we also examined the effects of proliferation on invasion and escape. Surprisingly, inhibiting proliferation enhanced the rate of invasion from the microtumors (Fig. 4). We therefore hypothesized that cells that initiate invasion are quiescent. Consistently, microtumors expressing the FUCCI reporter revealed that the majority of the cells that initiate invasions are in the G₀/G₁ phase of the cell cycle. Although blocking proliferation increases the rate at which invasion is initiated, we found that proliferation correlates with the extension of existing invasions. Invasion from the microtumors resembles angiogenic sprouting, wherein endothelial tip cells migrate and proliferate minimally, whereas stalk cells proliferate to support the extending vessel [65, 66]. Endothelial tip cells express high levels of vascular endothelial growth factor (VEGF) receptor, which in the presence of a VEGF gradient results in the formation and extension of filopodia to allow the initiation of sprouts [66]. Stalk cells, on the other hand, show high levels of Notch signaling, minimal filopodia, and high proliferation rates, thus allowing for sprout extension, growth, and branching [66]. Irradiating sprouting cells to inhibit proliferation permits some extension of the sprout before extension ceases [65], similar to the dynamics of invasion that we observe in mimosine-treated microtumors. These microtumors invade earlier than controls but show no differences in escape kinetics, highlighting the need for proliferation to sustain the extension of invasions. This behavior is reminiscent of the ability of irradiated endothelial cells to initiate vascular sprouts that eventually cease in their extension.

Recommended guidelines to treat solid tumors like those of the breast involve a cocktail of chemotherapeutics, many of which target cell proliferation. Given the high percentage

of recurrence observed in patients treated with these drugs, it is not surprising that we found inhibiting proliferation of the microtumors causes earlier invasion and still allows escape [67, 68]. The failure of these cytotoxic drugs to reduce tumor burden is often attributed to the heterogeneity of cancer cells and the presence of drug-resistant cells that do not respond to the therapy [67, 68]. Our data support an alternate explanation (Fig. 7): inhibiting proliferation leads to the upregulation of MMP expression, which suggests that tumors that are impervious to cell cycle inhibitors may potentially be explained by a change in phenotype rather than chemoresistance per se. Our findings suggest that chemotherapeutics, which aim to reduce tumor size and metastatic spread, would be more effective if optimized to target both the highly proliferative nature of tumors as well as the ability of their constituent cells to degrade and invade through the matrix microenvironment. In other words, antiproliferative agents and MMP inhibitors in combination may be more effective than either individually in the treatment of premetastatic breast cancer.

ABBREVIATIONS

EMT, epithelial–mesenchymal transition; ECM, extracellular matrix; MMP, matrix metalloproteinase; PCR, polymerase chain reaction; FUCCI, fluorescent ubiquitination-based cell cycle indicator; PDMS, polydimethylsiloxane; PBS, phosphate-buffered saline; cDNA, complementary DNA; ANOVA, analysis of variance; VEGF, vascular endothelial growth factor; ATCC, American Type Culture Collection; DMEM/F12, Dulbecco's modified Eagle medium/nutrient mixture F12; MEM, minimal essential medium; EdU, 5-ethynyl-2'-deoxyuridine; BLAST, basic local alignment search tool; DMSO, dimethyl sulfoxide.

ACKNOWLEDGEMENT

The authors thank Usman Ghani, Yoseph Dance, and the members of the Tissue Morphodynamics Group for their insightful comments.

FUNDING

This work was supported by a grant from the National Cancer Institute at the National Institutes of Health (U01 CA214292). E.M.R. was supported in part by a National Research Service

Award fellowship (GM134602) from the National Institute of General Medical Sciences at the National Institutes of Health.

SUPPLEMENTARY DATA

Supplementary data is available at *INTBIO Journal* online.

REFERENCES

- Clark AG, Vignjevic DM. Modes of cancer cell invasion and the role of the microenvironment. *Curr Opin Cell Biol* 2015;**36**:13–22.
- Panková K, Rösel D, Novotný M, et al The molecular mechanisms of transition between mesenchymal and amoeboid invasiveness in tumor cells. *Cell Mol Life Sci* 2010;**67**:63–71.
- Pandya P, Orgaz JL, Sanz-Moreno V. Modes of invasion during tumour dissemination. *Mol Oncol* 2017;**11**:5–27.
- John A, Tuszynski G. The role of matrix metalloproteinases in tumor angiogenesis and tumor metastasis. *Pathol Oncol Res* 2001;**7**:14–23.
- Heerboth S, Housman G, Leary M, et al EMT and tumor metastasis. *Clin Transl Med* 2015;**4**:6.
- Simi AK, Anlaş AA, Stallings-Mann M, et al A soft microenvironment protects from failure of midbody abscission and multinucleation downstream of the EMT-promoting transcription factor Snail. *Cancer Res* 2018;**78**:2277–89.
- Radisky ES, Radisky DC. Matrix metalloproteinases as breast cancer drivers and therapeutic targets. *Front Biosci (Landmark Ed)* 2015;**20**:1144–63.
- Gupta SC, Kim JH, Prasad S, et al Regulation of survival, proliferation, invasion, angiogenesis, and metastasis of tumor cells through modulation of inflammatory pathways by nutraceuticals. *Cancer Metastasis Rev* 2010;**29**:405–34.
- Hanahan D, Weinberg RA. The hallmarks of cancer. *Cell* 2000;**100**:57–70.
- Ewald AJ. An arresting story about basement membrane invasion. *Dev Cell* 2015;**35**:143–4.
- Gao CF, Xie Q, Su YL, et al Proliferation and invasion: plasticity in tumor cells. *Proc Natl Acad Sci U S A* 2005;**102**:10528–33.
- Kohrman AQ, Matus DQ. Divide or conquer: cell cycle regulation of invasive behavior. *Trends Cell Biol* 2017;**27**:12–25.
- Gallaher JA, Brown JS, Anderson ARA. The impact of proliferation-migration tradeoffs on phenotypic evolution in cancer. *Sci Rep* 2019;**9**:2425.
- Lehn S, Tobin NP, Berglund P, et al Down-regulation of the oncogene cyclin D1 increases migratory capacity in breast cancer and is linked to unfavorable prognostic features. *Am J Pathol* 2010;**177**:2886–97.
- DeMichele A, Yee D, Esserman L. Mechanisms of resistance to neoadjuvant chemotherapy in breast cancer. *N Engl J Med* 2017;**377**:2287–9.
- Karagiannis GS, Pastoriza JM, Wang Y, et al Neoadjuvant chemotherapy induces breast cancer metastasis through a TMEM-mediated mechanism. *Sci Transl Med* 2017;**9**:eaan0026.
- Keklikoglou I, Gianciarusio C, Guc E, et al Chemotherapy elicits pro-metastatic extracellular vesicles in breast cancer models. *Nat Cell Biol* 2019;**21**:190–202.
- Chiang SP, Cabrera RM, Segall JE. Tumor cell intravasation. *Am J Physiol Cell Physiol* 2016;**311**:C1–14.
- Cheon DJ, Orsulic S. Mouse models of cancer. *Annu Rev Pathol* 2011;**6**:95–119.
- Fantozzi A, Christofori G. Mouse models of breast cancer metastasis. *Breast Cancer Res* 2006;**8**:212.
- Day CP, Merlino G, Van Dyke T. Preclinical mouse cancer models: a maze of opportunities and challenges. *Cell* 2015;**163**:39–53.
- Gómez-Cuadrado L, Tracey N, Ma R, et al Mouse models of metastasis: progress and prospects. *Dis Model Mech* 2017;**10**:1061–74.
- Kim JB. Three-dimensional tissue culture models in cancer biology. *Semin Cancer Biol* 2005;**15**:365–77.
- Katt ME, Placone AL, Wong AD, et al In vitro tumor models: advantages, disadvantages, variables, and selecting the right platform. *Front Bioeng Biotechnol* 2016;**4**:12.
- Tien J, Truslow JG, Nelson CM. Modulation of invasive phenotype by interstitial pressure-driven convection in aggregates of human breast cancer cells. *PLoS One* 2012;**7**:e45191.
- Piotrowski-Daspit AS, Simi AK, Pang MF, et al A 3D culture model to study how fluid pressure and flow affect the behavior of aggregates of epithelial cells. *Methods Mol Biol* 2017;**1501**:245–57.
- Tien J, Dance YW, Ghani U, et al Interstitial hypertension suppresses escape of human breast tumor cells via convection of interstitial fluid. *Cell Mol Bioeng* in press.
- Tien J, Ghani U, Dance YW, et al Matrix pore size governs escape of human breast cancer cells from a microtumor to an empty cavity. *iScience* 2020;**23**:101673.
- Piotrowski-Daspit AS, Tien J, Nelson CM. Interstitial fluid pressure regulates collective invasion in engineered human breast tumors via Snail, vimentin, and E-cadherin. *Integr Biol (Camb)* 2016;**8**:319–31.
- Chary SR, Jain RK. Direct measurement of interstitial convection and diffusion of albumin in normal and neoplastic tissues by fluorescence photobleaching. *Proc Natl Acad Sci U S A* 1989;**86**:5385–9.
- Groebe K, Vaupel P. Evaluation of oxygen diffusion distances in human breast cancer xenografts using tumor-specific in vivo data: role of various mechanisms in the development of tumor hypoxia. *Int J Radiat Oncol Biol Phys* 1988;**15**:691–7.
- Forster JC, Harriss-Phillips WM, Douglass MJ, et al A review of the development of tumor vasculature and its effects on the tumor microenvironment. *Hypoxia (Auckl)* 2017;**5**:21–32.
- Awwad HK, el Naggat M, Mocktar N, et al Intercapillary distance measurement as an indicator of hypoxia in carcinoma of the cervix uteri. *Int J Radiat Oncol Biol Phys* 1986;**12**:1329–33.
- Oganesian A, Yarov-Yarovoy V, Parks WC, et al Constitutive coupling of a naturally occurring human alpha1a-adrenergic receptor genetic variant to EGFR transactivation pathway. *Proc Natl Acad Sci U S A* 2011;**108**:19796–801.
- Alessandri K, Sarangi BR, Gurchenkov VV, et al Cellular capsules as a tool for multicellular spheroid production and for investigating the mechanics of tumor progression in vitro. *Proc Natl Acad Sci U S A* 2013;**110**:14843–8.
- Gilbert DM, Neilson A, Miyazawa H, et al Mimosine arrests DNA synthesis at replication forks by inhibiting deoxyribonucleotide metabolism. *J Biol Chem* 1995;**270**:9597–606.
- Kubens BS, Niggemann B, Zänker KS. Prevention of entrance into G2 cell cycle phase by mimosine decreases locomotion of cells from the tumor cell line SW480. *Cancer Lett* 2001;**162**:S39–47.
- Mashanov VS, Zueva OR, García-Arrarás JE. Inhibition of cell proliferation does not slow down echinoderm neural regeneration. *Front Zool* 2017;**14**:12.
- Huebner RJ, Neumann NM, Ewald AJ. Mammary epithelial tubes elongate through MAPK-dependent coordination of cell migration. *Development* 2016;**143**:983–93.

40. Ju H, Hao J, Zhao S, et al Antiproliferative and antifibrotic effects of mimosine on adult cardiac fibroblasts. *Biochim Biophys Acta* 1998;**1448**:51–60.
41. Hegedüs L, Cho H, Xie X, et al Additional MDA-MB-231 breast cancer cell matrix metalloproteinases promote invasiveness. *J Cell Physiol* 2008;**216**:480–5.
42. Wang QM, Lv L, Tang Y, et al MMP-1 is overexpressed in triple-negative breast cancer tissues and the knockdown of MMP-1 expression inhibits tumor cell malignant behaviors. *Oncol Lett* 2019;**17**:1732–40.
43. Liu H, Kato Y, Erzinger SA, et al The role of MMP-1 in breast cancer growth and metastasis to the brain in a xenograft model. *BMC Cancer* 2012;**12**:583.
44. Köhrmann A, Kammerer U, Kapp M, et al Expression of matrix metalloproteinases (MMPs) in primary human breast cancer and breast cancer cell lines: new findings and review of the literature. *BMC Cancer* 2009;**9**:188.
45. Chen Z, Wu G, Ye F, et al High expression of MMP19 is associated with poor prognosis in patients with colorectal cancer. *BMC Cancer* 2019;**19**:448.
46. Yu G, Herazo-Maya JD, Nukui T, et al Matrix metalloproteinase-19 promotes metastatic behavior in vitro and is associated with increased mortality in non-small cell lung cancer. *Am J Respir Crit Care Med* 2014;**190**:780–90.
47. Ling B, Watt K, Banerjee S, et al A novel immunotherapy targeting MMP-14 limits hypoxia, immune suppression and metastasis in triple-negative breast cancer models. *Oncotarget* 2017;**8**:58372–85.
48. Di D, Chen L, Guo Y, et al Association of BCSC-1 and MMP-14 with human breast cancer. *Oncol Lett* 2018;**15**:5020–6.
49. Sakaue-Sawano A, Kurokawa H, Morimura T, et al Visualizing spatiotemporal dynamics of multicellular cell-cycle progression. *Cell* 2008;**132**:487–98.
50. Valastyan S, Weinberg RA. Tumor metastasis: molecular insights and evolving paradigms. *Cell* 2011;**147**:275–92.
51. Lim EJ, Suh Y, Kim S, et al Force-mediated proinvasive matrix remodeling driven by tumor-associated mesenchymal stem-like cells in glioblastoma. *BMB Rep* 2018;**51**:182–7.
52. Lu P, Takai K, Weaver VM, et al Extracellular matrix degradation and remodeling in development and disease. *Cold Spring Harb Perspect Biol* 2011;**3**:a005058.
53. Polacheck WJ, Charest JL, Kamm RD. Interstitial flow influences direction of tumor cell migration through competing mechanisms. *Proc Natl Acad Sci U S A* 2011;**108**:11115–20.
54. Polacheck WJ, German AE, Mammoto A, et al Mechanotransduction of fluid stresses governs 3D cell migration. *Proc Natl Acad Sci U S A* 2014;**111**:2447–52.
55. Duffy MJ. The role of proteolytic enzymes in cancer invasion and metastasis. *Clin Exp Metastasis* 1992;**10**:145–55.
56. Stamenkovic I. Matrix metalloproteinases in tumor invasion and metastasis. *Semin Cancer Biol* 2000;**10**:415–33.
57. Overall CM, López-Otín C. Strategies for MMP inhibition in cancer: innovations for the post-trial era. *Nat Rev Cancer* 2002;**2**:657–72.
58. Cathcart J, Pulkoski-Gross A, Cao J. Targeting matrix metalloproteinases in cancer: bringing new life to old ideas. *Genes Dis* 2015;**2**:26–34.
59. Winer A, Adams S, Mignatti P. Matrix metalloproteinase inhibitors in cancer therapy: turning past failures into future successes. *Mol Cancer Ther* 2018;**17**:1147–55.
60. Li K, Tay FR, Yiu CKY. The past, present and future perspectives of matrix metalloproteinase inhibitors. *Pharmacol Ther* 2020;**207**:107465.
61. Wolf K, Mazo I, Leung H, et al Compensation mechanism in tumor cell migration: mesenchymal-amoeoid transition after blocking of pericellular proteolysis. *J Cell Biol* 2003;**160**:267–77.
62. Taddei ML, Giannoni E, Morandi A, et al Mesenchymal to amoeoid transition is associated with stem-like features of melanoma cells. *Cell Commun Signal* 2014;**12**:24.
63. Parri M, Taddei ML, Bianchini F, et al EphA2 reexpression prompts invasion of melanoma cells shifting from mesenchymal to amoeoid-like motility style. *Cancer Res* 2009;**69**:2072–81.
64. Winer A, Janosky M, Harrison B, et al Inhibition of breast cancer metastasis by presurgical treatment with an oral matrix metalloproteinase inhibitor: a preclinical proof-of-principle study. *Mol Cancer Ther* 2016;**15**:2370–7.
65. Sholley MM, Ferguson GP, Seibel HR, et al Mechanisms of neovascularization. Vascular sprouting can occur without proliferation of endothelial cells. *Lab Invest* 1984;**51**:624–34.
66. Ribatti D, Crivellato E. “Sprouting angiogenesis”, a reappraisal. *Dev Biol* 2012;**372**:157–65.
67. Wind NS, Hoken I. Multidrug resistance in breast cancer: from in vitro models to clinical studies. *Int J Breast Cancer* 2011;**2011**:967419.
68. Luqmani YA. Mechanisms of drug resistance in cancer chemotherapy. *Med Princ Pract* 2005;**14**:35–48.

Supplementary material:

Table S1. Primers used for qRT-PCR analysis

Gene	Sequence
18S rRNA	Forward: CGGCGACGACCCATTCGAAC Reverse: GAATCGAACCCCTGATTCCCCGTC
MMP1	Forward: GACAGAAAGAGACAGGAGAC Reverse: GAGTTATCCCTTGCCTATCC
MMP14	Forward: GAGCTCAGGGCAGTGGATAG Reverse: GGTAGCCCCGGTTCTACCTTC
MMP19	Forward: GGGTCCTGTTCTTCCTACAT Reverse: CAATCCTGCAGTACTGGTCT

Figure S1. Cumulative frequency plots showing that microtumors were distance-matched. **(A)** Cumulative frequency plot showing that the two groups of microtumors treated with vehicle control or GM6001 in Fig. 2 were equally matched ($n = 32, 30, 30, 30$ for $D < 150 \mu\text{m}$ vehicle control, $D < 150 \mu\text{m}$ GM6001, $150 < D < 300 \mu\text{m}$ vehicle control, and $150 < D < 300 \mu\text{m}$ GM6001-treated microtumors, respectively). **(B)** Cumulative frequency plot showing that the two groups of microtumors treated with vehicle control ($n = 26$) or GM6001 ($n = 21$) in Fig. 2 were equally matched. **(C)** Cumulative frequency plot showing that the two groups of microtumors treated with vehicle control ($n = 26$) or mimosine ($n = 26$) in Fig. 4 were equally matched.

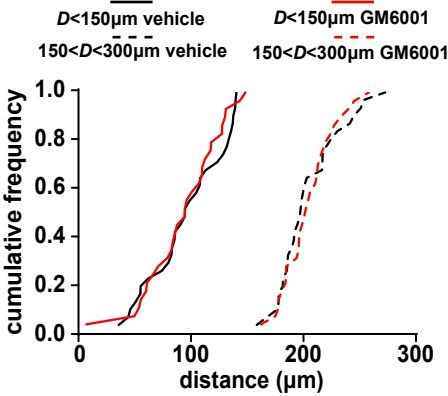
Figure S2. EdU analysis of microtumors treated with vehicle control or mimosine. Shown are mean \pm s.d. of three independent experiments. *** $P < 0.001$ using Student's t-test.

Figure S3. Inhibiting proliferation by treating with aphidicolin leads to earlier invasion. **(A)** Timeline of experiment. **(B)** Phase-contrast images of microtumors treated with vehicle control (DMSO) (*top panel*) or the DNA-replication inhibitor aphidicolin (*bottom panel*). **(C)**

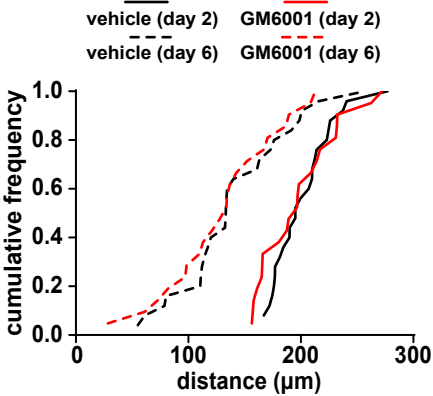
Cumulative frequency plot showing that the two groups of microtumors treated with vehicle control ($n = 36$) or aphidicolin ($n = 40$) were distance-matched. **(D)** EdU analysis of microtumors treated with vehicle control or aphidicolin. Kaplan-Meier plots of **(E)** invasion ($P < 0.0001$, HR: 4.4, 95% CI: 2.2-8.8) and **(F)** escape ($P = 0.69$) for microtumors treated with vehicle control ($n = 30$) or aphidicolin ($n = 29$). Shown are mean \pm s.d. of 3-4 independent experiments. *** $P < 0.001$ using Student's t-test (D). Scale bar, 200 μm .

Figure S1

A



B



C

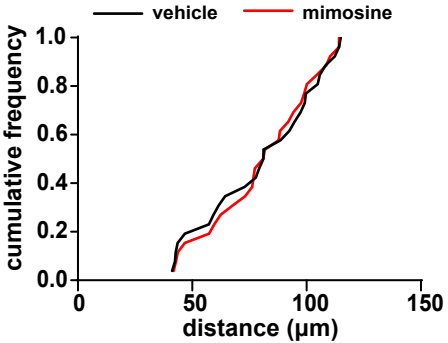


Figure S2

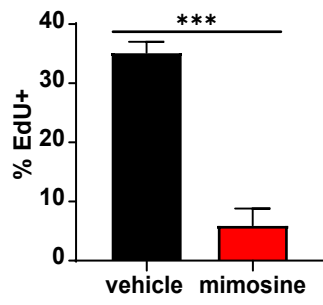
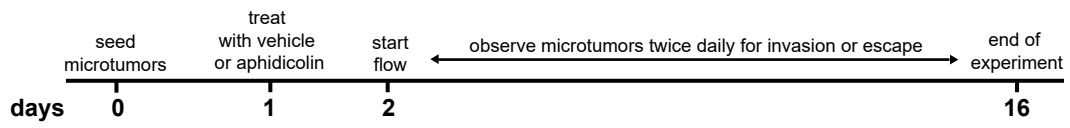
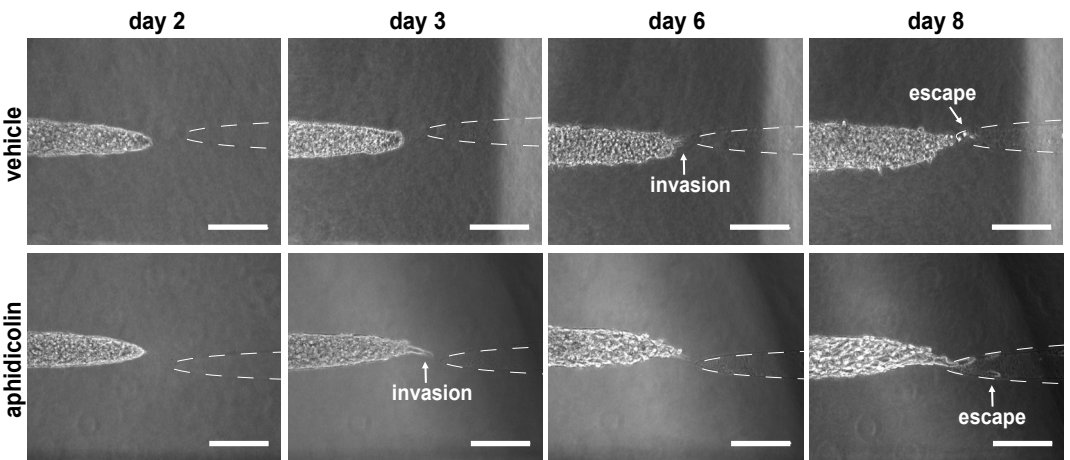


Figure S3

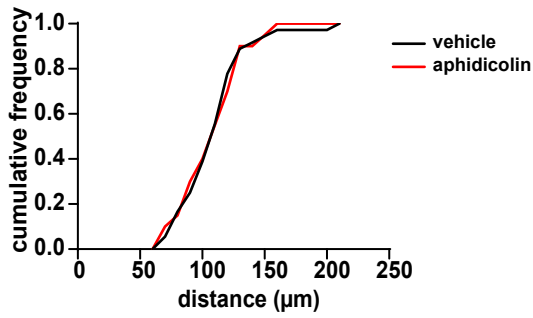
A



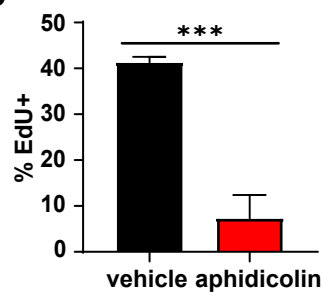
B



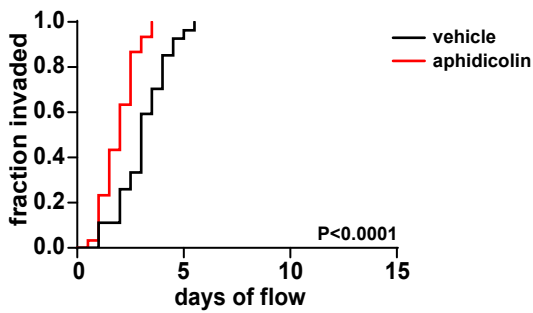
C



D



E



F

